BARYON STOPPING AND ASSOCIATED PRODUCTION OF MESONS IN Au+Au COLLISIONS AT $\sqrt{s_{NN}} = 3.0$ GeV AT STAR*

Benjamin Kimelman

for the STAR Collaboration

University of California, Davis
1 Shields Ave, Davis, CA 95616, USA

Received 28 July 2022, accepted 21 September 2022, published online 14 December 2022

In these proceedings, we present the first measurements of identified charged hadrons in Au+Au collisions at $\sqrt{s_{NN}} = 3.0$ GeV. Results of baryon stopping, associated production of kaons, and the Coulomb potential of stopped protons are presented. Physics implications of these measurements are discussed.

DOI:10.5506/APhysPolBSupp.16.1-A49

1. Introduction

Relativistic heavy-ion collisions are a prime tool to probe the phase structure of strongly interacting matter under extreme conditions. The RHIC Beam Energy Scan II (BES-II) program has three primary goals: searching for the onset of the Quark–Gluon Plasma (QGP), studying the properties of the produced QCD matter, and locating the possible QCD phase boundary and critical endpoint [1].

Particle production has long been used to investigate the properties of the produced QCD matter in heavy-ion collisions. The BES-II program covers a wide range of energies, including the transition from a hadronic dominated medium to a partonic dominated one, which has been predicted to occur around $\sqrt{s_{NN}} = 7.7$ GeV [2]. The BES-II program was designed to improve and extend upon the results from the BES-I program. Of particular interest is the high baryon density region which is accessible through the STAR fixed-target program that extends the energy reach from $\sqrt{s_{NN}} = 7.7$ GeV

* Presented at the 29$^{\text{th}}$ International Conference on Ultrarelativistic Nucleus–Nucleus Collisions: Quark Matter 2022, Kraków, Poland, 4–10 April, 2022.

to $\sqrt{s_{NN}} = 3.0$ GeV. In these proceedings, the first measurements of charged particle production in Au+Au collisions at $\sqrt{s_{NN}} = 3.0$ GeV are presented. These data were collected in 2018 and contain 275 M minimum-bias events.

2. Charged hadron spectra

Charged hadron spectra are obtained using a combination of data from the Time Projection Chamber (TPC) and barrel Time of Flight (bTOF). The specific energy loss ($\mathrm{d}E/\mathrm{d}x$) can be obtained from the TPC and the mass squared (m^2) can be obtained from the bTOF, both of which are binned in rapidity (y), transverse mass ($m_\mathrm{T} - m_0$), and centrality. Each bin is fit with multiple Gaussian distributions to determine the yield of the particle of interest while accounting for contamination from other particle species.

Invariant yields are obtained after correcting for the limited detector acceptance and efficiency, which are obtained by embedding simulated tracks, after passing through the Geant simulation of the detector response, into real data. Pion spectra are fit with a double thermal function in order to extrapolate to the unmeasured region at low $m_\mathrm{T} - m_0$; the same fit function was used by the E895 experiment to describe the pion production from the Δ-resonance at low $m_\mathrm{T} - m_0$ and thermal production at high $m_\mathrm{T} - m_0$ [3]. Kaons are fit with an m_T-exponential function to extrapolate to low $m_\mathrm{T} - m_0$, which assumes that enhancement effects due to the Bose–Einstein statistics are mostly canceled out by suppression effects from the radial flow. Proton spectra are fit with a Blast-Wave model [4] which describes the radial expansion of the fireball assuming a cylindrical expansion. By integrating the yields over the measured $m_\mathrm{T} - m_0$ region and extrapolating to low $m_\mathrm{T} - m_0$, the rapidity density distributions ($\mathrm{d}N/\mathrm{d}y$) are obtained.

3. Particle production

In low-energy collisions, particle production of hadrons has various different mechanisms and can be affected by the final-state effects. In this section, we discuss the Coulomb potential and its effect on the pion spectra, the ratio of K^-/K^+ and its implications for different hadron production mechanisms, and measurements of baryon stopping.

3.1. Coulomb potential

The Coulomb potential of the fireball, while small, can affect the momenta distributions of charged hadrons. This effect will be most evident for the charged pions as they are the lightest hadrons. Additionally, the Coulomb potential should affect positively- and negatively-charged pions in

opposite ways: shifting π^+ to higher $m_T - m_0$ and π^- to lower $m_T - m_0$. By taking a ratio of π^+/π^- as a function of $m_T - m_0$, the Coulomb potential can be extracted using a model fit. The model incorporates the Bose–Einstein nature of pions and an effective potential to account for the momentum distribution of stopped protons [5] (which will be discussed further in Sec. 3.3). An example fit of the pion ratio with this model can be seen in Fig. 1 (a). From this fit, the Coulomb potential (V_C) and initial pion ratio (R_{init}) can be extracted. The same procedure can be applied to all centralities to obtain the Coulomb potential, which has been plotted against the midrapidity proton dN/dy for each corresponding centrality bin in Fig. 1 (b). The two curves represent power law fits, following a similar study done by the HADES Collaboration [6], indicating the source is non-spherical.

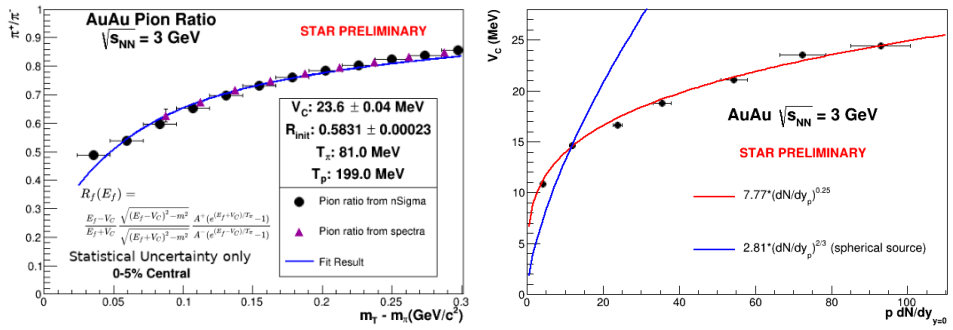

(a) (b)

Fig. 1. (Color online) (a) Ratio of π^+/π^- at midrapidity in central Au+Au collisions at $\sqrt{s_{NN}} = 3.0$ GeV. The pion ratio is fit with a model accounting for the Bose–Einstein nature of pions and an effective potential to account for the momentum distribution of stopped protons [5]. (b) Coulomb potential extracted from the pion ratio at midrapidity plotted against the midrapidity proton dN/dy for the corresponding centrality bins. Power law fits are performed with free parameters (red/gray) and with the power fixed based on a spherical source assumption (blue/black), indicating the source is non-spherical.

3.2. Associated production of kaons

Production of kaons is more difficult than pions due to their strangeness content. K^+ (which contain an $\bar{s}$ quark) can be produced in association with a Λ baryon ($N + N \to N + \Lambda + K$), which is more energetically favorable compared to pair production ($N + N \to N + N + K + K$); however, both production mechanisms are available for K^+. K^- (which contain an s quark) will not be produced via this associated mechanism as it would require the

production of a $\bar{\Lambda}$, which requires much more energy; therefore, K^- are only produced in pairs with the K^+. The ratio of K^-/K^+ indicates the fraction of K^+ that are produced in pairs with the K^-, with the remainder being produced in association with a Λ baryon. Figure 2 shows this ratio at midrapidity as a function of collision energy, which follows the trend seen in previous measurements [7–11]. It also shows that approximately 5% of K^+ are produced in a pair with a K^-, while the remaining 95% are produced in association with a Λ baryon at $\sqrt{s_{NN}} = 3.0$ GeV.

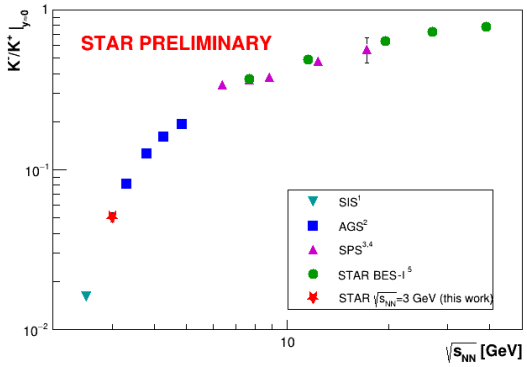

Fig. 2. Ratio of K^-/K^+ at midrapidity in central collisions. This ratio indicates the fraction of K^+ produced in pairs with a K^-, which is only about 5% at $\sqrt{s_{NN}} = 3.0$ GeV, and approaches unity for higher-energy collisions. The remaining K^+ are produced in association with a Λ baryon.

3.3. Baryon stopping

Baryon stopping occurs when participating nucleons interact with each other and lose energy in the form of rapidity. Measurements of this rapidity loss provide a straightforward way to quantify the amount of stopping. Figure 3 (a) shows the proton dN/dy distribution for all centralities, which exhibits a clear trend of the peak shifting from midrapidity in central collisions to beam/target rapidity in peripheral collisions, indicating a change in the baryon stopping. Figure 3 (b) shows the proton dN/dy in 0–5% central collisions, which is fit with two-mirrored peaks determined by counting the number of collisions each participating nucleon takes part in a Monte Carlo Glauber models, and smoothed using a Gaussian kernel. Stopping (δy) is defined as the shift of the projectile participant peak from beam rapidity, as demonstrated in Fig. 3 (b).

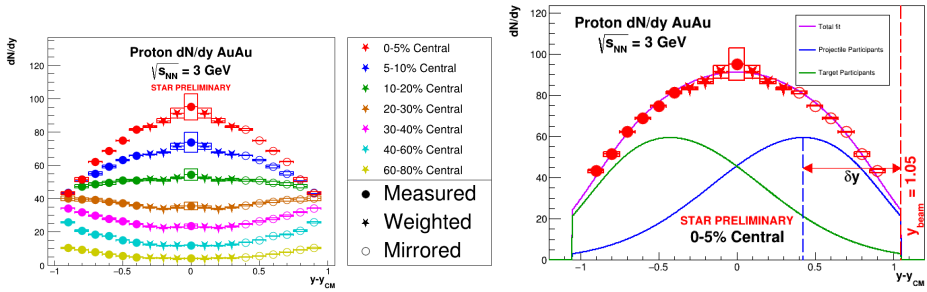

(a) (b)

Fig. 3. (Color online) (a) Proton dN/dy for all centralities. The change in shape, with the peak shifting from midrapidity toward beam/target rapidity from central to peripheral collisions, indicates a change in the baryon stopping. (b) Proton dN/dy in central collisions fit with two mirrored peaks representing the projectile (blue/black) and target (green/gray) participants. The stopping, δy, is defined as the shift of the projectile participant peak from beam rapidity.

The amount of stopping is obtained for all centrality classes and plotted in Fig. 4 against the average number of binary collisions divided by the average number of participants divided by two ($\frac{\langle N_{\rm Coll}\rangle}{\langle N_{\rm part}\rangle/2}$) for the corresponding centrality class. This can be used to estimate the average rapidity loss of a nucleon for each binary collision. In central and mid-central collisions, a clear linear trend exists which, when fit with a line, has a slope of 0.19, indicating that in these centrality classes, each binary nucleon–nucleon collision

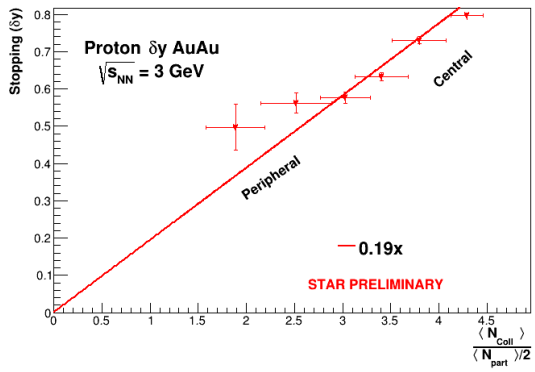

Fig. 4. Baryon stopping (δy) plotted against the average number of binary collisions per participant for all centrality classes. The linear trend in central and mid-central collisions indicates a constant average rapidity loss per binary collision of 0.19±0.01 units. Peripheral collisions being above this average may indicate a larger rapidity loss from the first binary collision.

causes an average loss of 0.19 ± 0.01 units of rapidity. In contrast, peripheral collisions fall above this linear trend, indicating each binary collision causes a larger rapidity loss. This could be explained by the first binary collision having a higher $\sqrt{s_{NN}}$ compared to successive ones which, therefore, would cause a larger loss of rapidity. In these peripheral collisions where each nucleon undergoes very few binary collisions, we are perhaps seeing the larger impact of the first binary collision, which gets averaged out with more binary collisions seen in central collisions.

4. Summary

Spectra of identified $\pi^{\pm}$, $K^{\pm}$, and p have been measured in Au+Au fixed-target collisions at $\sqrt{s_{NN}} = 3.0$ GeV with STAR. The final-state Coulomb potential has been measured using the ratio of π^+/π^-, which plotted against the proton $\mathrm{d}N/\mathrm{d}y$ indicates that the source of the potential is non-spherical. The ratio of K^-/K^+ has been measured and indicates that only 5% of K^+ are produced thermally in pairs with K^-, and the remaining 95% are produced in association with the Λ baryon. Finally, baryon stopping has been measured using protons and indicates that each participant has an average loss of 0.19 units of rapidity per nucleon–nucleon collision in central and mid-central collisions, whereas peripheral collisions have a higher average rapidity loss, possibly due to a larger rapidity loss from the first binary collision.

REFERENCES

[1] STAR Collaboration, «Studying the Phase Diagram of QCD matter», 2014.

[2] J. Randrup, J. Cleymans, *Phys. Rev. C* **74**, 047901 (2006).

[3] E895 Collaboration (J.L. Klay *et al.*), *Phys. Rev. C* **68**, 054905 (2003).

[4] E. Schnedermann, J. Sollfrank, U. Heinz, *Phys. Rev. C* **48**, 2462 (1993).

[5] D. Cebra *et al.*, arXiv:1408.1369 [nucl-ex].

[6] HADES Collaboration (J. Adamczewski-Musch *et al.*), *Eur. Phys. J. A* **58**, 166 (2022), arXiv:2202.12750 [nucl-ex].

[7] A. Förster *et al.*, *J. Phys. G: Nucl. Part. Phys.* **28**, 2011 (2002).

[8] E866 Collaboration (L. Ahle *et al.*), *Phys. Lett. B* **490**, 53 (2000).

[9] NA49 Collaboration (C. Alt *et al.*), *Phys. Rev. C* **77**, 024903 (2008).

[10] NA49 Collaboration (S.V. Afanasiev *et al.*), *Phys. Rev. C* **66**, 054902 (2002).

[11] STAR Collaboration (L. Adamczyk *et al.*), *Phys. Rev. C* **96**, 044904 (2017).